The 2.0 Å crystal structure of a heterotrimeric G protein

David G. Lambright*†, John Sondek*, Andrew Bohm*, Nikolai P. Skiba‡, Heidi E. Hamm‡ & Paul B. Sigler*§

* The Department of Molecular Biophysics and Biochemistry, and the Howard Hughes Medical Institute, Yale University, 295 Congress Avenue, BCMM 154, New Haven, Connecticut 06510, USA
‡ Department of Physiology and Biophysics, University of Illinois at Chicago, Chicago, Illinois 60680, USA

The structure of a heterotrimeric G protein reveals the mechanism of the nucleotide-dependent engagement of the α and βγ subunits that regulates their interaction with receptor and effector molecules. The interaction involves two distinct interfaces and dramatically alters the conformation of the α but not of the βγ subunits. The location of the known sites for post-translational modification and receptor coupling suggest a plausible orientation with respect to the membrane surface and an activated heptahelical receptor.

MANY extracellular signals are mediated by heptahelical receptors coupled to heterotrimeric guanine-nucleotide-binding proteins (G protein; subunits, $\alpha\beta\gamma$)[1–3]. In response to diverse stimuli, including light, hormones and neurotransmitters, heptahelical receptors activate heterotrimeric G proteins by catalysing the exchange of GTP for GDP bound to the G_α subunit. An agonist-stimulated receptor activates as many as several hundred G proteins, which in turn activate a variety of downstream effectors including enzymes, ion channels[4], and intracellular signalling pathways such as the MAP kinase cascade[5,6]. In the resting state, the GDP form of the G_α subunit (G_αGDP) forms a high-affinity (nM) complex with the $G_{\beta\gamma}$ heterodimer. Binding of the heterotrimeric complex to an agonist-activated receptor results in the release of GDP. Subsequent GTP binding disrupts the complex with the receptor and leads to the dissociation of G_αGTP from $G_{\beta\gamma}$. Both activated G_αGTP and the released $G_{\beta\gamma}$ subunits are free to interact with downstream components of the signalling cascade. As a consequence of an intrinsic GTPase activity in the G_α subunit, GTP is hydrolysed to GDP, thereby returning the system to its heterotrimeric resting state.

One of the best characterized heterotrimeric G-protein-coupled pathways is the visual cascade of the rod cell[7,8], where the light-activated heptahelical receptor, rhodopsin, couples to the heterotrimeric G protein transducin ($G_{t\alpha\beta\gamma}$). $G_{t\alpha}$GTP activates a potent cyclic GMP phosphodiesterase by displacing its inhibitory γ-subunits. A comparison of the structure of $G_{t\alpha}$ complexed with either GDP[9] or GTP-γS[10] (a non-hydrolysable GTP analogue) revealed the nucleotide-dependent structural changes that distinguish the GTP-bound (active) form from the GDP-bound (inactive) form. The structural changes occurring within the G_α subunit are not global, but rather are restricted to three adjacent 'switch' regions. Highly localized rearrangements within the context of an otherwise active GTP-bound conformation stabilize the transition state for GTP hydrolysis[11,12].

We now describe the refined 2.0 Å crystal structure of a heterotrimeric G-protein complex. A comparison with the previously determined $G_{t\alpha}$GDP structure[9] and that of free $G_{t\beta\gamma}$ (ref. 26) establishes the conformational changes that occur in each subunit to form the heterotrimer interface and hence reveals the mechanism of GTP-induced release and activation of $G\beta\gamma$. The sites of post-translational modification on $G_{t\alpha}$ and $G_{t\gamma}$ combined with the receptor-binding regions of $G_{t\alpha}$, deduced from biochemical studies, occur on a common face that orients the heterotrimer with respect to the membrane surface.

Structure determination and refinement

A modified heterotrimeric complex of transducin was prepared by mixing endo-Lys-C-proteolysed $G_{t\beta\gamma}$ with a $G_{t\alpha}/G_{i\alpha1}$ chimaera ($G_{t\alpha/i\alpha1}$) in which residues 216–294 of $G_{t\alpha}$ were replaced with the corresponding residues (220–298) from $G_{i\alpha1}$ (ref. 13). This chimaera binds guanine nucleotides, assumes an active conformation in the presence of aluminium fluoride, and interacts with $G_{t\beta\gamma}$ and rhodopsin in a light-dependent manner[13]. Proteolysis of $G_{t\beta\gamma}$ with endo-Lys-C removes only the farnesyl modification and three residues from the C terminus of $G_{t\gamma}$ while leaving $G_{t\beta}$ intact. $G_{t\alpha/i\alpha1}$ was expressed in *Escherichia coli* as a soluble fusion with an N-terminal 6xHis tag which was not removed before crystallization. Diffraction-quality crystals of the heterotrimeric complex in the monoclinic space group *C*2 were grown as described (Table 1).

The structure was solved at 3.0 Å by multiple isomorphous replacement (MIR) using isomorphous differences from a $Hg(OAc)_2$ derivative and isomorphous as well as single-wavelength anomalous differences from a CH_3HgCl derivative and a selenomethionine (SeMet) derivative substituted in the $G_{t\alpha/i\alpha1}$ subunit. The intial map was improved with solvent flattening and histogram matching. A molecular replacement (MR) solution for the $G_{t\alpha/i\alpha1}$ subunit was obtained at 4 Å using the $G_{t\alpha}$GDP structure as a search model. Although the phases obtained from the MR solution were not sufficiently accurate to generate an interpretable map of the protein, they were useful for calculating derivative difference Fourier maps which allowed the location of heavy atom sites in each of the derivatives. Using Sigma A weights to reduce model bias, an interpretable map was calculated at 3.0 Å resolution with phases derived from multiple isomorphous replacement and anomalous scattering combined with phases from the partially refined molecular replacement model.

The model was refined with simulated annealing against the SeMet intensities from 6.0 to 2.0 Å resolution (Table 1). The present model includes residues 6–343 for $G_{t\alpha/i\alpha1}$, residues 2–340 for $G_{t\beta\gamma}$, residues 8–66 for $G_{t\gamma}$, a GDP molecule, 630 water molecules, and has an *R* value of 20.7% for all data (19.6% for data $>2\sigma$) and a free *R* value of 29.5% (28.4% for data $>2\sigma$) for a randomly selected subset (10%) of the data omitted before the start of refinement. An example of the $2F_o - F_c$ electron density map is shown in Fig. 2*d*. The structure has

† Present address: Program in Molecular Medicine, University of Massachusetts Medical Center, 373 Plantation Street, Worcester, Massachusetts 01605, USA.
§ To whom correspondence should be addressed.

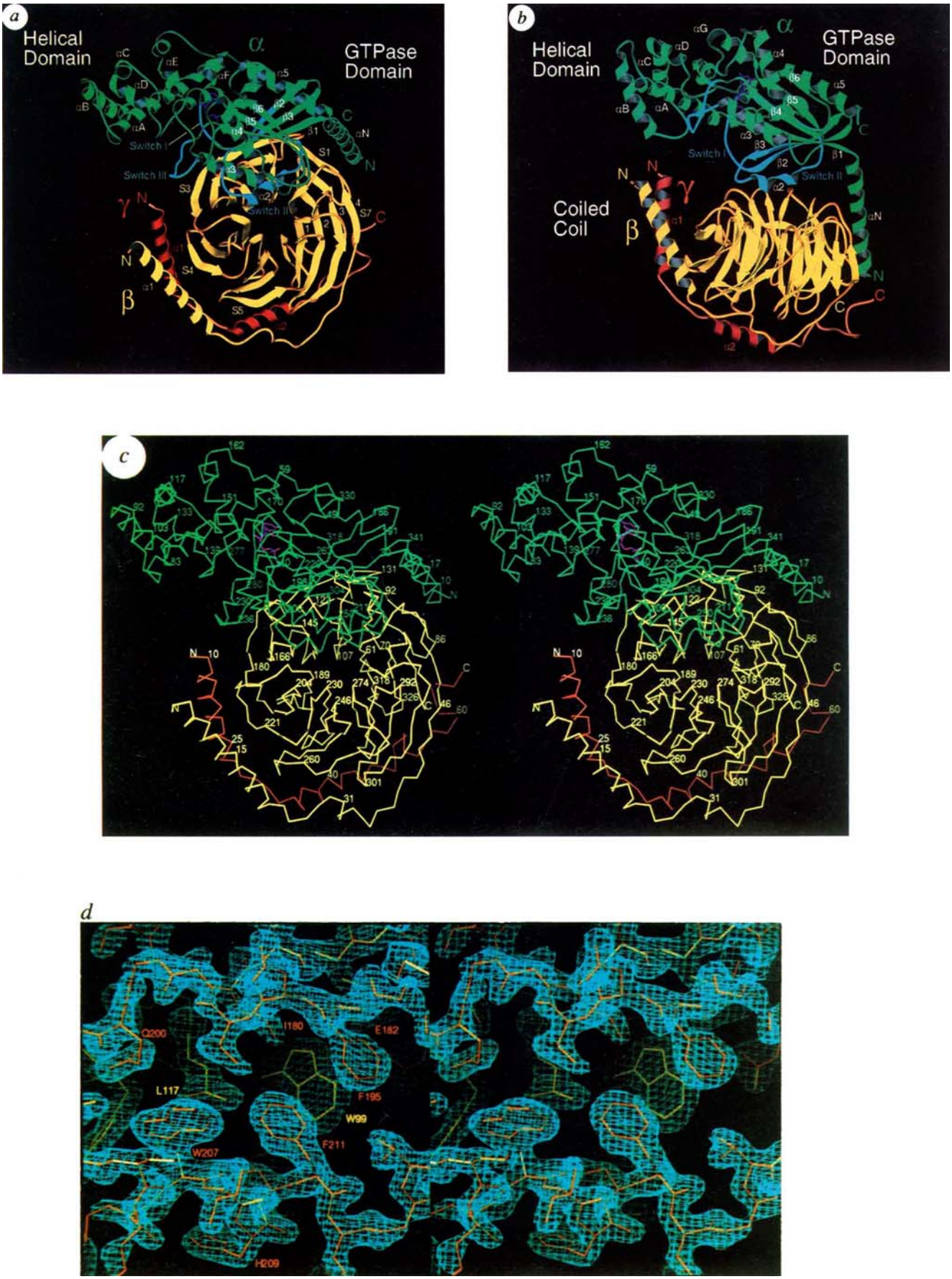
a
Helical Domain
GTPase Domain
Switch I
Switch II
Switch III
b
Helical Domain
GTPase Domain
Coiled Coil
Switch I
Switch II
c
d
Q200
I180
E182
L117
F195
W99
W207
F211
H209

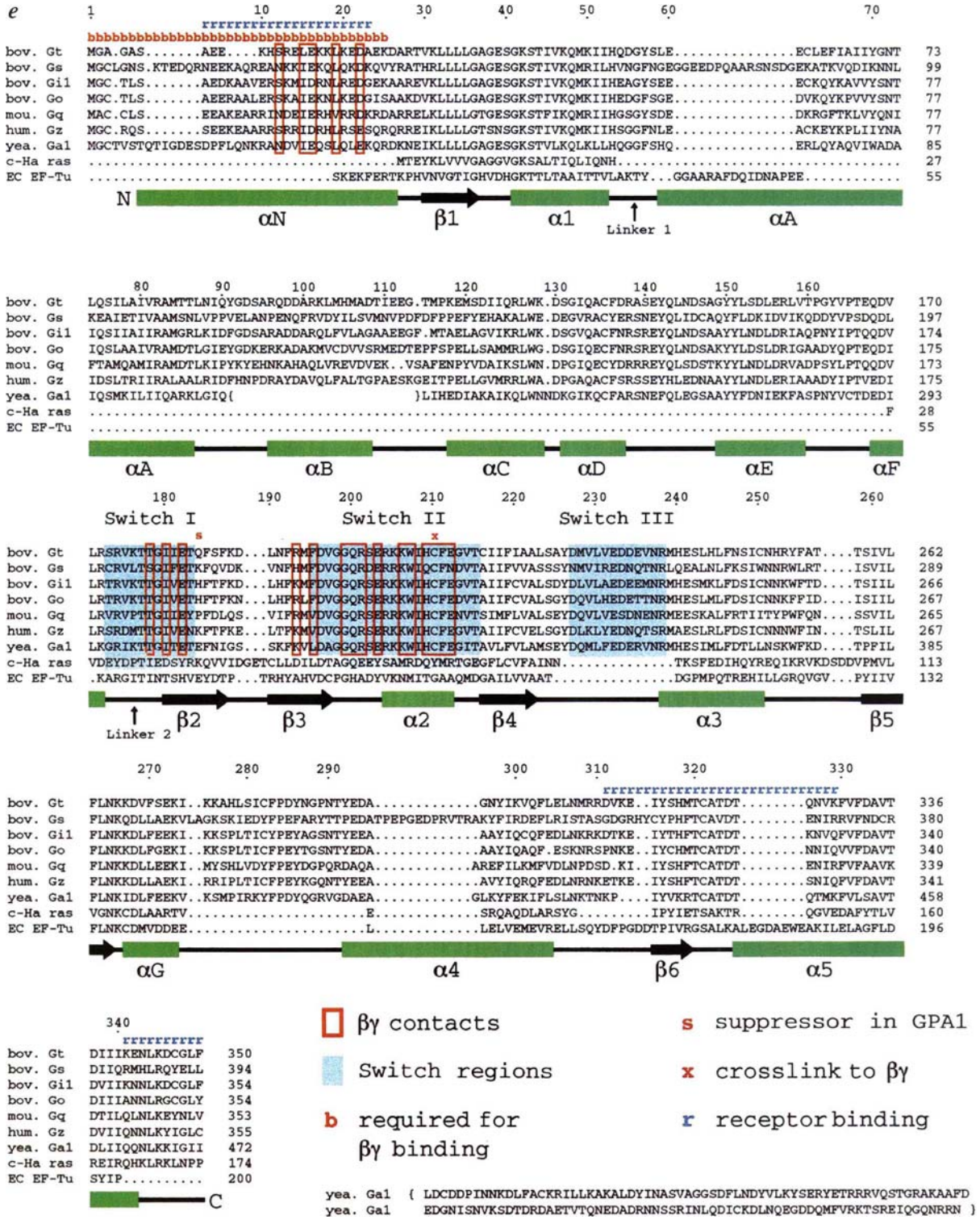

FIG. 1 Structure of the $G_{t\alpha/i\alpha}G_{t\beta\gamma}$ heterotrimeric complex with $G_{t\alpha/i\alpha}$ shown in green, $G_{t\beta}$ in yellow, $G_{t\gamma}$ in red, GDP in magenta, and the switch I–III regions of $G_{t\alpha/i\alpha}$ in cyan. *a*, Ribbon drawing of the complex viewed down the axis of the β-propeller domain of $G_{t\beta\gamma}$. *b*, Ribbon drawing of the complex rotated 70° about the horizontal axis compared with the view in *a*. *c*, Stereo pair showing the Cα atoms of the complex oriented as in *a*. *d*, $2F_{obs} - F_{calc}$ electron-density map contoured at 1.5σ showing residues in the switch interface. *e*, Sequence alignment for G_{α} subunits with the secondary structure corresponding to $G_{t\alpha/i\alpha}$ shown below the aligned sequences. Residues that contact $G_{t\beta}$ are indicated with red boxes and residues in the switch regions are highlighted in light blue. Also indicated are residues that have been implicated as in or near the $G_{\beta\gamma}$ and receptor binding regions based on biochemical experiments and yeast genetics.

excellent stereochemistry and ϕ–ψ angles within allowed regions of the Ramachandran plot. A more detailed description of the structure solution and refinement is given in the legend of Table 1.

Overall structure

The structure of the heterotrimeric $G_{t\alpha/i\alpha}GDP \cdot G_{t\beta\gamma}$ complex is depicted in Fig. 1. The $G_{t\alpha}$ subunit has three distinct structural components: (1) a Ras-like GTPase domain consisting of a six-stranded β-sheet surrounded by six helices ($\alpha1$–$\alpha5$ and αG); (2) an entirely α-helical domain consisting of a long central helix (αA) surrounded by 5 shorter helices (αB–αF); and (3) an N-terminal helix (αN) that projects away from the remainder of the $G_{t\alpha}$ subunit. The guanine nucleotide binds tightly in a deep cleft between the GTPase and helical domains. In general, the helical and GTPase domains as well as the guanine nucleotide closely resemble their counterparts in $G_{t\alpha}GDP$, except for significant changes where the GTPase domain contacts $G_{t\beta\gamma}$. The N-terminal helix could not be observed in previously determined $G_{t\alpha}$ structures[9–11] where it was removed by proteolysis and was disordered in the structure of $G_{i\alpha1}GTP\gamma S$[12]. The conformation of the N-terminal helix does not resemble that observed in the crystal structure of $G_{i\alpha1}GDP$[14].

The $G_{t\beta}$ subunit has an N-terminal helix followed by a repeating module of seven similar β-sheets, each with four antiparallel strands, that form the 'blades' of a β-propeller structure (Fig. 1*a*). The outside strand of each sheet, together with the inner three strands of the following sheet, comprise the structural unit corresponding to the 'WD'-sequence repeat first noted in $G_{t\beta}$[15]. The $G_{t\gamma}$ subunit contains two helices and has no inherent tertiary structure. The N-terminal helix of $G_{t\gamma}$ forms a coiled-coil with the N-terminal helix of $G_{t\beta}$ whereas the remainder of $G_{t\gamma}$ interacts extensively with the β-propeller domain of $G_{t\beta}$. The details of the $G_{t\beta\gamma}$ structure are described in an accompanying paper[26].

G_α interactions with $G_{\beta\gamma}$

As shown in Fig. 2*a*, the interaction between the $G_{t\alpha}$ and $G_{t\beta\gamma}$ subunits occurs at two distinct interfaces. The most extensive interface involves residues in, or adjacent to, the switch I and II regions of $G_{t\alpha}$ that interact with residues from loops and turns at the top of the β-propeller domain of $G_{t\beta}$. The second interface is formed between the N-terminal helix of $G_{t\alpha}$ and the side of the β-propeller domain of $G_{t\beta}$. We shall refer to the former as the 'switch interface' because it involves regions of $G_{t\alpha}$ that have been shown previously to undergo nucleotide dependent conformational changes and the latter as the 'N-terminal interface' because it involves only the N-terminal helix of $G_{t\alpha}$.

The switch interface buries ~1,800 Å^2 of solvent-accessible surface area and includes residues from $\beta2$, $\beta3$, and $\alpha2$ in $G_{t\alpha}$ as well as residues from five of the seven sheets in $G_{t\beta}$. Fig. 2*b* shows the core of this tightly packed interface which consists of the side chains from six hydrophobic residues in $G_{t\alpha}$ (Ile 180, Phe 195, Trp 207, His 209, Cys 210 and Phe 211) and four hydrophobic residues in $G_{t\beta}$ (Tyr 59, Trp 99, Met 101 and Leu 117). The interaction is further stabilized by a network of hydrophilic interactions including both main-chain and side-chain hydrogen bonds and is flanked by two ion pairs. The specific interactions are shown schematically in Fig. 2*g*.

In contrast, only ~900 Å^2 of solvent-accessible surface area is buried in the N-terminal interface. As depicted in Fig. 2*c*, five residues on one side of the N-terminal helix of $G_{t\alpha}$ (Ser 12, Glu 16, Leu 19, Asp 22 and Ala 23) interact with four residues from the first sheet of $G_{t\beta}$ (Leu 55, Lys 78, Ile 80, Lys 89). The conserved Lys 89 plays an essential role through a tripartite interaction in which its backbone NH donates a hydrogen bond to the hydroxyl group of Ser 12 while its methylene groups pack against the side chains of Leu 15 and Leu 19 thereby positioning its amino group to form an ion pair with the carboxylate group of Glu 16. In addition to enhancing the stability of the complex, the N-terminal interface also determines the location of the modified N terminus of G_α.

In contrast to extensive interactions with $G_{t\beta}$, no direct interactions are observed between $G_{t\alpha}$ and $G_{t\gamma}$. However, the first five residues of $G_{t\alpha}$ as well as the first eight and last four residues of $G_{t\gamma}$ are disordered. Therefore, the absence of interactions between $G_{t\alpha}$ and $G_{t\gamma}$ in the present structure does not rule out the possibility that such interactions might occur under a more physiological setting. However, the extent of such an interaction would be limited.

Numerous biochemical and mutational studies have implicated the N terminus and switch II regions of G_α in the interaction with $G_{\beta\gamma}$. Limited proteolysis[16], a monoclonal antibody directed against the N terminus[17,18], and expression of N-terminally truncated G_α subunits[19,20] indicate that the myristoylated N terminus and some portion of the first 25 residues of G_α are essential for high-affinity binding to $G_{\beta\gamma}$. The ability of $G_{o\alpha}$ to be ADP-ribosylated at Cys 351 by pertussis toxin is impaired by mutations at residues corresponding to Lys 17 and Lys 31 in $G_{t\alpha}$[21]. Both residues are exposed to solvent and neither contacts $G_{t\beta}$, suggesting that they may contribute to interactions with the toxin and/or the negatively charged membrane surface. The Gly 226 to alanine mutation in $G_{s\alpha}$ that disrupts the GTP-induced conformational changes in the switch II region also blocks the release of $G_{\beta\gamma}$[22,23], consistent with the extensive interaction between $G_{t\beta}$ and the switch regions of $G_{t\alpha}$. Finally, the conserved Cys 215 in the switch II region of $G_{o\alpha}$ can be crosslinked by a 15 Å divalent alkylating agent to either of two conserved cysteines in $G_{t\beta}$ (Cys 204 and Cys 271)[24]. The crosslinks are compatible with the location of these cysteine residues in the structure (see Fig. 2*e*).

Regions of G_β that contact G_α have been implicated by yeast genetics. Mutational changes in the yeast mating factor G_β (ste4p) at residues corresponding to Trp 99 and Met 101 in $G_{t\alpha}$ (Fig. 2*e*) cause constitutive activation of the pheromone signalling pathway and are defective for interaction with the yeast mating factor G_α (GPA1) in the yeast two-hybrid assay[25]. Strikingly exposed on the surface of free $G_{t\beta\gamma}$, these residues lie at the core of the hydrophobic switch interface with $G_{t\alpha}$ in the heterotrimeric complex (Fig. 2*b*). In addition, some of the constitutively active mutants in the yeast G_β can be suppressed by a second site revertant (E307K)[25] at a residue corresponding to Gln 184 in $G_{t\alpha}$, which lies at the edge of the switch interface. Inspection of the heterotrimer structure predicts that a lysine residue at this position would be situated to form an ion pair with a non-conserved aspartic acid residue (Asp 133 in yeast G_β) located at the position of Arg 96 in $G_{t\beta}$.

Most of the contacts involve residues that are highly conserved in both G_α (Fig. 1*e*) and G_β (see accompanying paper[26]). Substitutions at these positions are typically conservative even in sequences from distantly related organisms. It is therefore likely that the interactions observed here can be generalized to other members the heterotrimeric G-protein family. Moreover, the structure does not reveal an obvious basis for specificity in the pairing of particular G_α and $G_{\beta\gamma}$ subunits. Thus, the extent to which specificity is determined at the level of the G_α interaction with $G_{\beta\gamma}$ or at the level of the heterotrimer interaction with the receptor remains an interesting question.

Conformational changes in G_α

Figure 3 shows a superposition of the previously determined structures of free $G_{t\alpha}GDP$[9] and $G_{t\alpha}GTP\gamma S$[10] onto that of $G_{t\alpha}GDP$ in the heterotrimeric complex. The overall conformation is preserved except for residues within the switch I and II regions and a few flexible loops. The differences between the free and heterotrimeric forms of $G_{t\alpha}GDP$ are most pronounced for residues that interact with $G_{t\beta}$ directly. Some of these are critically conserved residues that are important to the structure and function of $G_\alpha GTP$, such as Gly 199 which triggers conformational changes in the switch II region through an interaction with the γ phosphate in the GTP[9,10], and Gln 200 which stabilizes the transition state for GTP hydrolysis[11,12].

The most dramatic changes occur in the switch II region. In free

$G_{t\alpha}$GDP, the β3 strand terminates in a tight turn (Gly 198–Gln 200) that precedes the α2 helix (Arg 201 to His 209). As opposed to the taut and compact GTP-bound form, the α2 helix in free $G_{t\alpha}$GDP is a loosely configured 3_{10} helix with conserved hydrophobic and polar residues exposed and accessible to proteases. In order to engage the $G_{t\beta}$ subunit, the residues from Gly 198 to Ser 202 adopt an extended conformation, allowing the remainder of the α2 helix to swing outwards, exposing and positioning residues to interact with $G_{t\beta}$. As a consequence, the hydrogen-bonding network between the β2 and β3 strands is extended at the expense of that between β3 and β1. These changes do not significantly alter the solvent-accessibility of the nucleotide. However, it is likely that $G_{\beta\gamma}$ binding stabilizes the otherwise flexible switch I and II regions, perhaps accounting for the

TABLE 1 Structure determination and refinement

Crystal	Source	Data collection Resolution limit (Å)	R_{sym} (%)*	% Complete
Native	*R*-axis II	2.5	7.2	97
SeMet	NSLS X25	2.1	6.1	99
MeHgCl	*R*-axis II	3.5	9.1	85
$Hg(OAc)_2$	Xentronics	3.4	11.2	87

MIR phasing statistics

Resolution limit (Å)	16.90	10.17	7.27	5.66	4.63	3.92	3.40	3.00	Overall
Phasing power†‡ SeMet	0.32	0.63	0.54	0.53	0.38	0.28	0.23	0.23	0.30
SeMet (anomalous)	0.21	0.24	0.30	0.32	0.28	0.28	0.25	0.21	0.26
$Hg(OAc)_2$	1.14	1.71	1.90	2.33	1.67	1.16	0.95	–	1.42
MeHgCl	1.42	1.58	1.79	2.41	1.93	1.34	0.95	–	1.55
MeHgCl (anomalous)	0.05	0.27	0.36	0.30	0.23	0.15	0.07	–	0.16
Mean figure of merit	0.43	0.57	0.56	0.54	0.46	0.36	0.23	0.13	0.31

Rotation search

Search model	Euler angles Θ_1	Θ_2	Θ_3	Refined PC (Ω) § Highest peak	Highest false peak
$G_{t\alpha}$GDP	29.3	88.7	42.7	15.7σ	5.5σ

Translation search

Space group	Fractional coordinates *x*	*y*	*z*	Translation function %§ Highest peak	Highest false peak
*C*2	0.21	0.00	0.15	21σ	16σ

	Resolution (Å)	Refinement *R* factor	Free *R* factor	No. of reflections
Data with $F > 2\sigma$	6–2.0	19.6	28.4	49,438
All data	6–2.0	20.7	29.5	54,174
R.m.s. deviations		Bond lengths 0.01Å Bond angles 1.5°		

$G_{t\alpha\beta\gamma}$ was isolated from photolysed bovine retinal rod outer segments (ROS) by selective extraction with GTP[49] and the subunits separated by chromatography on Cibracon blue Sepharose as described[9]. $G_{t\beta\gamma}$ was proteolysed with 10 U of the lysine-specific protease endo-Lys C for 12 hours at 4 °C followed by cation exchange chromatography on Mono-Q (10 mM Tris, pH 7.5, 0.1–0.2 M NaCl gradient over 30 column volumes). The $G_{t\alpha/i\alpha}$ chimaera was expressed as a soluble 6xHis fusion in *E. coli* as described[13]. Diffraction-quality crystals of the heterotrimeric complex were grown in microseeded hanging drops containing 10 mg ml^{-1} protein, 10% PEG-8000, 50 mM Tris, pH 8.0, 10% glycerol, 50 mM NaCl and 0.1% β-mercaptoethanol over a well containing the identical solution without the protein. Crystals appeared in 1–2 days and grew to a maximum of 0.3 × 0.3 × 0.5 mm in 1 week. The space group is *C*2 with unit cell dimensions of $a = 133.4$, $b = 91.4$, $c = 83.2$ Å. Crystals were incubated for 12 h at 4 °C in a cryoprotectant stabilizer solution containing 30% PEG-8000, 10% glycerol, 50 mM Tris, pH 8.0. The Hg^{2+} and CH_3Hg^+ derivatives were obtained by soaking in the presence of 0.1 mM mercuric acetate and 1 mM CH_3HgCl respectively. Crystals were flash-frozen in liquid propane which was cooled with liquid nitrogen. The native and CH_3Hg^+ derivative data sets were collected at −150 °C on an *R* axis II image plate system and processed with DENZO (Z. Otwinowski). The Hg^{2+} derivative data set was collected at 100K on a Xentronics area detector and processed with XDS[50]. Diffraction data for the Se-methionine derivative were collected at 100K at the peak of the Se absorption edge at the X-25 beamline of the National Synchrotron Light Source at Brookhaven, processed with DENZO (Z. Otwinowski). All data sets were scaled with SCALEPACK (Z. Otwinowski). The location of the $G_{t\alpha/i\alpha1}$ subunit was found by molecular replacement using as a search model the $G_{t\alpha}$GDP structure in which residues in the range of the chimera were truncated to alanine. A rotation search using Patterson correlation refinement[51] resulted in a single solution. A translation search yielded a clear solution with an *R* value of 50.5% after rigid-body refinement. Heavy-atom sites were located from isomorphous and anomalous differences Fouriers with phases calculated from the molecular replacement solution for the $G_{t\alpha}$ subunit. The coordinates and occupancies of the heavy atoms were refined with ML-PHARE. Initial MIR phases were improved by solvent flattening, histogram matching, and partial model combination using DPHASE (G. van Duyne). All computations for molecular replacement and subsequent refinement were carried out with X-PLOR 3.1 (ref. 52). Interactive model building was done with O (ref. 53).

* $R_{sym} = \Sigma|I_h - \langle I_h\rangle|\Sigma I_h$.

† Phasing power $= \Sigma|F_H|/\Sigma\|F_{PH}obs| - |F_{PH}calc\|$.

‡ Anomalous phasing power $= \Sigma|F''_H|/\Sigma\|ADobs| - |ADcalc\|$.

§ $$\%PC(\Omega) = \frac{\left\langle |E_{obs}|^2 |E_m(\Omega)|^2 - \langle |E_{obs}|^2 \rangle \langle |E_m(\Omega)|^2 \rangle \right\rangle}{\left[\left\langle |E_{obs}|^4 - \langle |E_{obs}|^2 \rangle^2 \right\rangle \left\langle |E_m(\Omega)|^4 - \langle |E_m(\Omega)|^2 \rangle^2 \right\rangle \right]^{1/2}},$$

where E_{obs} denotes the normalized observed structure factors and E_m denotes the normalized structure factors for the search model place in a triclinic unit cell with geometry identical to that of the crystal[33].

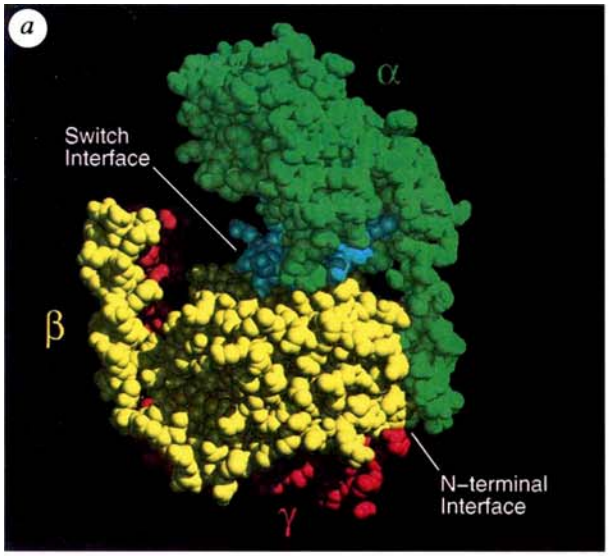

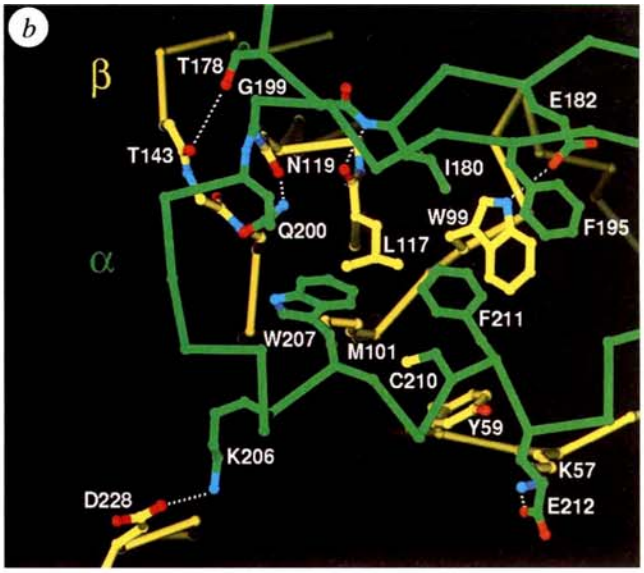

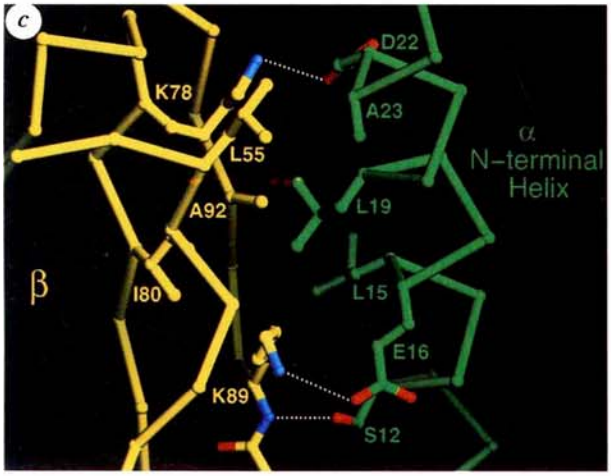

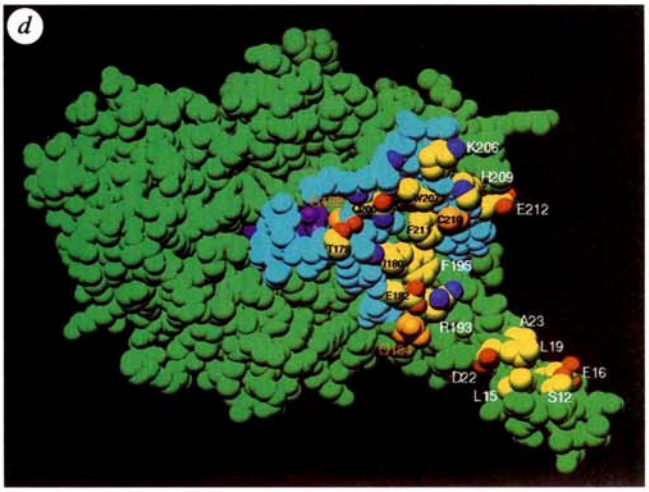

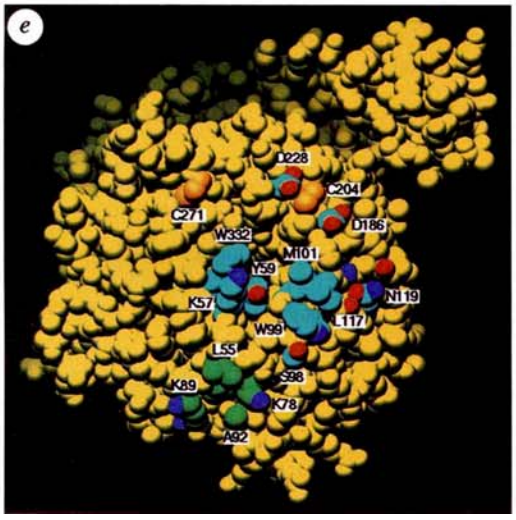

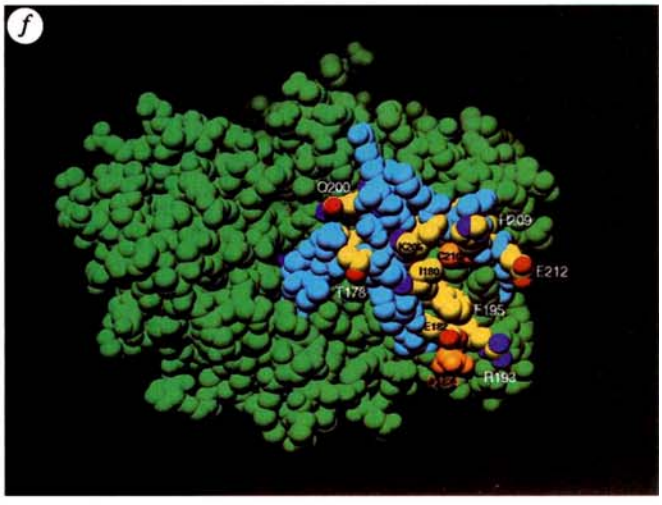

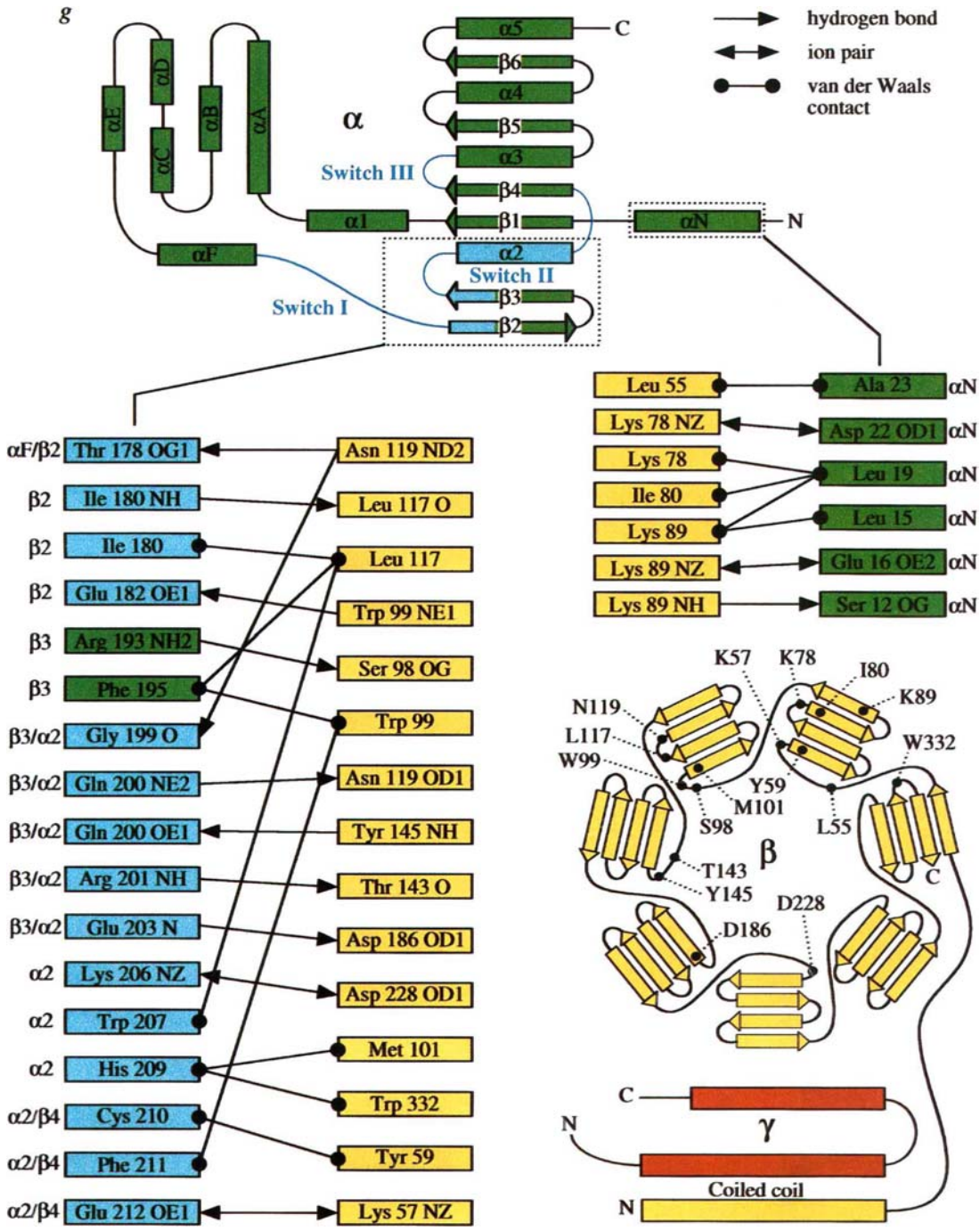

FIG. 2 Contacts in the two independent heterotrimer interfaces. *a*, Space-filling model showing the two distinct interfaces between the $G_{t\alpha}$ and $G_{t\beta\gamma}$ subunits. *b*, Ball-and-stick model of the switch interface showing α-carbons (green $G_{t\alpha}$; yellow in $G_{t\beta}$) and selected side chains (green in $G_{t\alpha}$ and yellow in $G_{t\beta}$, except for oxygens and nitrogens which are red and blue, respectively). *c*, Ball-and-stick model of the N-terminal interface showing α-carbons and selected side chains coloured as in *a*. *d*, Space-filling model of $G_{t\alpha/i\alpha}$GDP (green) showing the switch I and II regions (cyan) and the residues that contact $G_{t\beta}$ (yellow, except oxygens and nitrogens which are red and blue, respectively). View is similar to the canonical orientation described previously[9–11]. Residues identified in biochemical or mutational studies are highlighted in orange. *e*, Space-filling model of $G_{t\beta\gamma}$ (yellow) showing the residues that contact $G_{t\alpha/i\alpha}$GDP (green, except oxygens and nitrogens which are red and blue, respectively) in the switch interface. View is rotated by 180° about the *y*-axis compared to *d*. Residues corresponding to Trp 99 and Met 101 have been implicated by yeast genetics[25] as essential for the interaction between G_{α} and $G_{\beta\gamma}$. Two cysteines in G_{β} (Cys 204 and Cys 271) that can be chemically crosslinked to Cys 215 in $G_{o\alpha}$ (Cys 210 in $G_{t\alpha}$)[24] are indicated in orange. Cys 210 lies at the edge of the switch II interface and makes van der Waals contact with Tyr 59 in $G_{t\beta}$. At a distance of 13 Å from Cys 210, Cys 204 is located in a turn between the second and third strands of the fourth WD repeat and make van der Waals contact with the methylene groups of Lys 206 in $G_{t\alpha}$. Cys 271, on the other hand, occurs in the loop connecting the outer and inner strands of the sixth WD repeat and lies at a distance of 18 Å from Cys 210 and 10 Å from edge of the switch interface. *f*, Space-filling model of $G_{t\alpha}GTP\gamma S$ (coloured and oriented as in *d*) showing how the switch interface is disrupted by the GTP-induced conformational changes. *g*, Diagram of the interactions between $G_{t\alpha/i\alpha}$GDP and $G_{t\beta}$ in the heterotrimeric complex.

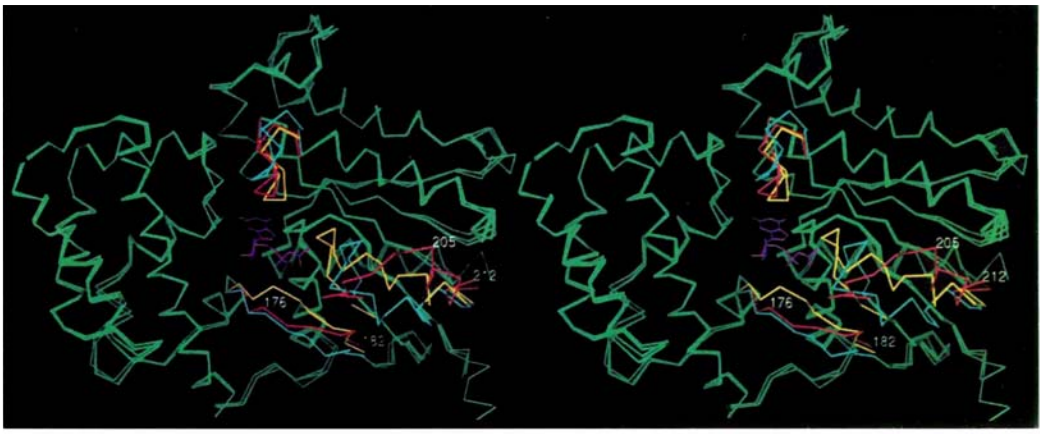

FIG. 3 Structural changes in $G_{t\alpha}$ and $G_{t\beta\gamma}$ subunits. Stereo pair showing the least-squares superimposed Cα traces of free $G_{t\alpha}$GDP, heterotrimeric $G_{t\alpha/i\alpha}$GDP, and $G_{t\alpha}$GTPγS oriented as in Fig. 1*a*. All three molecules are coloured green except for the switch I and II regions, which are blue for free $G_{t\alpha}$GDP, red for heterotrimeric $G_{t\alpha/i\alpha}$GDP, and yellow for $G_{t\alpha}$GTPγS.

observation that the interaction with $G_{\beta\gamma}$ decreases the rate of GDP release[27]. On replacement of GDP with GTP, local but dramatic conformational changes disrupt nearly all of the contacts in the switch interface, thereby triggering the disengagement of G_α and $G_{\beta\gamma}$. It is also likely that the structure of the N-terminal helix of G_α depends on the interaction with G_β, as its conformation in the heterotrimer differs markedly from that observed in the $G_{i\alpha}$GDP structure[14].

Implications

In contrast to the dramatic structural reorganization in the switch I and II regions of $G_{t\alpha}$, significant structural changes are not observed in $G_{t\beta\gamma}$. Although the structures of $G_{t\beta\gamma}$ alone and bound to $G_{t\alpha}$ were independently determined, the r.m.s. deviation in Cα positions after superposition is only 0.72 Å. Thus, the $G_{t\beta\gamma}$ subunits appear to function as a rigid unit with critical residues prepositioned to interact with $G_{t\alpha}$GDP or other signalling components. Whereas G_α activation proceeds through nucleotide-dependent structural reorganization, activation of $G_{\beta\gamma}$ occurs solely as a consequence of its release. This implies that the G_α subunit acts as a negative regulator of $G_{\beta\gamma}$ by restricting its degrees of freedom and/or masking sites on the surface of G_β that interact with downstream signalling components. The regions of yeast $G_{\beta\gamma}$ that interact with downstream signalling components have been mapped genetically[54,57]. None of the residues implicated in these studies lie within either of the two interfaces between G_α and $G_{\beta\gamma}$. Instead, they map to the coiled-coil and a region immediately adjacent to the switch interface (Fig. 3 of accompanying paper[26]). However, as both G_α and effectors are large macromolecules, steric constraints will extend the masked region of G_β beyond the actual van der Waals contact surface, thereby extending the effective 'footprint' of G_α on $G_{\beta\gamma}$. Thus the G_α and effector binding sites on $G_{\beta\gamma}$ need not overlap directly. In this respect, the helical domain of G_α (Fig. 1*b*) appears to be positioned such that it could sterically hinder the access of effectors that bind to regions similar to those implicated for yeast $G_{\beta\gamma}$.

Both the G_α and G_γ subunits undergo post-translational modification, resulting in the covalent attachment of specific lipophilic groups. The G_γ subunits are farnesylated ($G_{\gamma 1}$)[28,29] or geranyl geranylated ($G_{\gamma 2-4}$)[30–32] at the cysteine in the C-terminal CAAX motif. Several G_α subunits are subject to N-terminal myristoylation ($G_{i\alpha}$, $G_{o\alpha}$, $G_{z\alpha}$)[33] or heterogeneous acylation ($G_{t\alpha}$)[34,35] at Gly 2 and most (except $G_{t\alpha}$) are regulated by reversible palmitoylation at Cys 3[36,37]. These modifications are essential for membrane association. In addition, myristoylation of G_α[38] and prenylation of G_γ increase the stability of the heterotrimer complex[39]. Experiments with $G_{t\alpha}$ indicate that this stabilization occurs only in the presence of membranes or detergent micelles, suggesting that the primary role of the lipophilic modifications is to co-localize and orient the subunits on the membrane surface[40].

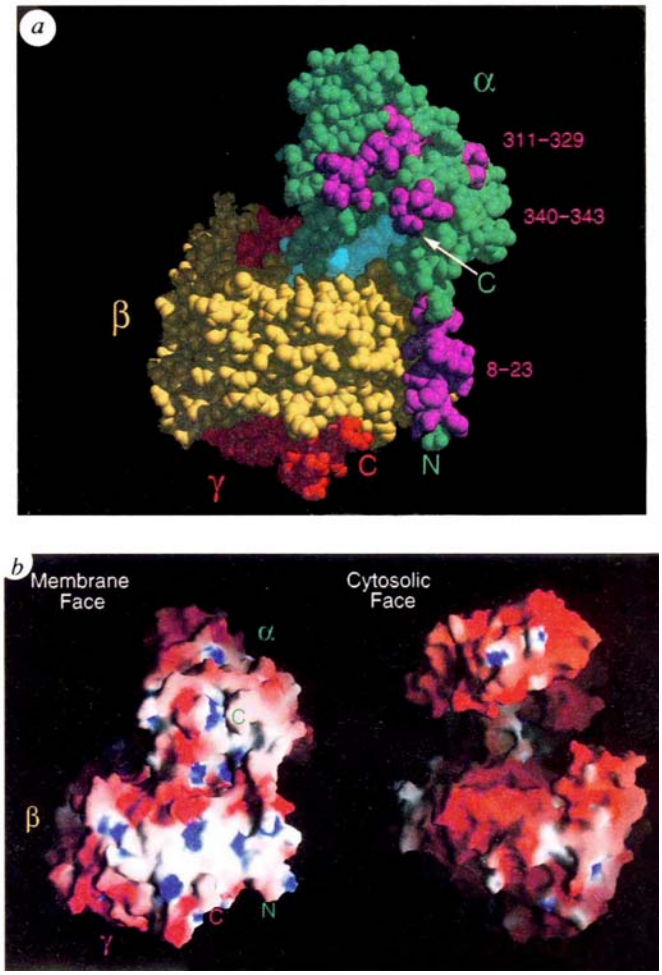

FIG. 4 Face of the heterotrimeric complex that is proposed to interact with the membrane surface and photoactivated rhodopsin. *a*, Space-filling model highlighting the sites of hydrophobic post-translational modification (N terminus of $G_{t\alpha}$ and C terminus of $G_{t\gamma}$) and regions that are known from biochemical experiments to contact receptors (purple). The orientation is rotated about the vertical axis by ~70° with respect to the view in Fig. 1*b*. *b*, Solvent-accessible surface coloured according to electrostatic potential using GRASP[56]. The electrostatic potential is contoured in the range from $-10\,k_BT$ (red) to $+10\,k_BT$ (blue) where k_B is Boltzmann's constant and T is the absolute temperature (K).

Although the G_α and G_γ subunits in this study lack these modifications, their sites of attachment can be approximated from the location of the unmodified N- and C-termini of G_α and G_γ respectively. In the present structure, the first four residues (Gly-Ala-Gly-Ala) from the N terminus of $G_{t\alpha}$ and the last four residues (Lys-Gly-Gly-Cys) from the C terminus of $G_{t\gamma}$ are not observed. The amino-acid sequences suggest that both regions could be conformationally flexible in the absence of other interactions. Moreover, the structures of $G_{t\alpha}$ and $G_{t\beta\gamma}$ do not reveal obvious binding sites for large hydrophobic groups. Significantly, the observed N terminus of $G_{t\alpha}$ and the observed C terminus of $G_{t\gamma}$ are located 18 Å apart on a common face of the heterotrimer. Thus, the structure is consistent with the hydrophobic modifications inserting simultaneously and cooperatively into the lipid bilayer rather than binding to sites on the protein and also supports the conclusion that the enhanced stability of the heterotrimer complex results from co-localization of the subunits to membranes or detergent micelles.

The receptor binding surface of G_α has been mapped approximately by biochemical and mutational data. Many experiments indicate that the C terminus of G_α is an essential region for receptor coupling. ADP ribosylation by pertussis toxin[41], mutations[42,43] and peptide-specific antibodies[44], all directed at the C terminus, uncouple G proteins from receptors. Experiments with G_α chimaeras indicate that this region is also important in determining G-protein receptor specificity[45]. A peptide corresponding to the C-terminal 11 amino acids has been shown to interact directly with photoactivated rhodopsin[46,47]. In addition, the C-terminal peptide and peptides corresponding to the end of the $\alpha 4/\beta 6$ loop through the beginning of $\alpha 5$ (residues 311–329) as well as most of the N-terminal helix (residues 8–23) inhibit G_t binding to rhodopsin[47].

The approximate locations of the sites of post-translational modification and receptor coupling occur on a common face of the heterotrimeric complex (Fig. 4*a*). This side of $G_{t\beta\gamma}$ is surprisingly flat, and electrostatic calculations reflect a predominantly neutral surface interspersed with patches of positive charge, in contrast to the other faces where the electrostatic potential is dominated by negatively charged residues (Fig. 4*b*). Thus, a plausible model would orient this face of the heterotrimer against the negatively charged membrane surface allowing the hydrophobic modifications to insert simultaneously into the lipid bilayer while positioning the known receptor contact sites of G_α to interact with an activated heptahelical receptor. In addition, $G_{t\beta\gamma}$ has also been shown to interact directly with rhodopsin[48]; however, the regions that contact the receptor have not been identified. One possible receptor contact site on $G_{t\beta}$, consistent with the location of the approximate receptor contact regions of G_α (Fig. 4*a*), is the region adjacent to the switch and N-terminal interfaces. The observation that $G_{\beta\gamma}$ interacts with both the receptor and the switch I/switch II region of G_α, which flanks the nucleotide binding site and buttresses the critical phosphate binding loop, gives stereochemical support to a potential role for $G_{\beta\gamma}$ in receptor-catalysed nucleotide exchange. In addition, the presence of receptor contact sites on both G_α and $G_{\beta\gamma}$ makes the stability of the receptor–G protein complex dependence dependent on the interaction between the subunits, and hence provides a simple mechanism for coupling the GTP-triggered dissociation of G_α and $G_{\beta\gamma}$ to their release from the receptor.

Ultimately, a mechanistic understanding of the nucleotide-exchange process will require the structure of an activated heptahelical receptor bound to the nucleotide free form of a heterotrimeric G protein. In the interim, the present study provides the basis for mutational experiments designed to test specific hypotheses regarding the mechanism of nucleotide exchange and better define the role of $G_{\beta\gamma}$ in facilitating this process.

Note added in proof: After this paper was submitted, Wall *et al.* (*Cell* **83,** 1047–1058, 1995) published a partially refined structure of $G_{i\alpha 1\beta 1\gamma 2}$ showing a similar overall architecture. However, a comparison of the intersubunit contacts of the G_t heterotrimer with those of the G_i heterotrimer is compromised by an admitted lack of 'atomicity' in the $G_{i\alpha 1\beta 1\gamma 2}$ model. □

Received 1 December; accepted 18 December 1995.

1. Conklin, B. R. & Bourne, H. R. *Cell* **73,** 631–641 (1993).
2. Neer, E. J. *Cell* **80,** 249–257 (1995).
3. Simon, M. I., Strathmann, M. P. & Gautam, N. *Science* **252,** 802–808 (1991).
4. Hepler, J. R. & Gilman, A. G. *Trends biochem. Sci.* **17,** 383–387 (1992).
5. Crespo, P., Xu, N., Simonds, W. F. & Gutkind, J. S. *Nature* **369,** 418–420 (1994).
6. Faure, M., Voyno-Yasenetskaya, A. & Bourne, H. R. *J. biol. Chem.* **269,** 7851–7854 (1994).
7. Hurley, J. B. *J. Bioenerg. Biomem.* **24,** 219–226 (1992).
8. Pfister, C. *et al. Cell Sig.* **5,** 235–241 (1993).
9. Lambridght, D. G., Noel, J. P., Hamm, H. E. & Sigler, P. B. *Nature* **369,** 621–628 (1994).
10. Noel, J. P., Hamm, H. E. & Sigler, P. B. *Nature* **366,** 654–663 (1993).
11. Sondek, J. S., Lambright, D. G., Noel, J. P., Hamm, H. E. & Sigler, P. B. *Nature* **372,** 276–279 (1994).
12. Coleman, D. E. *et al. Science* **265,** 1405–1412 (1994).
13. Skiba, N. *et al. J. biol. Chem.* **271,** 413–424 (1996).
14. Mixon, M. B. *et al. Science* **270,** 954 (1995). **(Initial?)**
15. Neer, E. J., Schmidt, C. J., Nambudripad, R. & Smith, T. F. *Nature* **371,** 297–300 (1994).
16. Fung, B. K. & Nash, C.R. *J. biol. Chem.* **258,** 10503–10510 (1983).
17. Mazzoni, M.R. & Hamm, H. E. *Biochemistry* **28,** 9873–9880 (1989).
18. Mazzoni, M. R., Malinski, J. A. & Hamm, H. E. *J. biol. Chem.* **266,** 14072–14081 (1991).
19. Graf, R., Mattera, R., Codina, J., Estes, M. K. & Birnbaumer, L. *J. biol. Chem.* **267,** 24307–24314 (1992).
20. Denker, B. M., Neer, E. J. & Schmidt, C. *J. biol. Chem.* **267,** 6272–6277 (1992).
21. Slepak, V. Z., Wilkie, T. M. & Simon, M. I. *J. biol. Chem* **268,** 1414–1423 (1993).
22. Miller, R.T. *et al. Nature* **267,** 712–715 (1988).
23. Lee,E., Taussig, R. & Gilman, A. G. *J. biol. Chem.* **267,** 1212–1218 (1992).
24. Garcia-Higuera, I., Thomas, T. C., Yi, F. & Neer, E. J. *J. biol. Chem.* **271,** 528 (1996).
25. Whiteway,M., Clark, K. L., Leberer, E., Dignard, D. & Thomas, D. Y. *Molec. cell. Biol.* **14,** 3223–3229 (1994).
26. Sondek, J., Bohm, A., Lambright, D. G., Hamm, H. E. & Sigler, P. B. *Nature* **379,** 369–374 (1996).
27. Higashijima, T., Ferguson, K. M., Sternweis, P. C., Murray, D. S. & Gilman, A. G. *J. biol. Chem.* **262,** 762–766 (1987).
28. Fukada, Y. *et al. Nature* **346,** 658–660 (1990).
29. Lai, R. K., Dolores, P.-S., Canada, F. J. & Rando, R. R. *Proc. natn. Acad. Sci. U.S.A.* **87,** 7673–7677 (1990).
30. Mumby, S. M., Casey, P. J., Gilman, A. G., Gutowski, S. & Sternweis, P. C. *Proc. natn. Acad. Sci. U.S.A.* **87,** 5873–5877 (1990).
31. Yamane, H. K. *et al. Proc. natn. Acad. Sci. U.S.A.* **87,** 5868–5872 (1990).
32. Maltese, W. A. & Robishaw, J. D. *J. biol. Chem.* **265,** 18071–18074 (1990).
33. Buss, J. E., Mumbry, S. M., Casey, P. J., Gilman, A. G. & Sefton, B. M. *Proc. natn. Acad. Sci. U.S.A.* **84,** 7493–7497 (1987).
34. Kokame, K., Fukada, Y., Yoshizawa, T., Takao, T. & Shimonishi, Y. *Nature* **359,** 749–752 (1992).
35. Neubert, T. A., Johnson, R. S., Hurley, J. B. & Walsh, K. A. *J. biol. Chem.* **267,** 18274–18277 (1992).
36. Linder, M. E. *et al. Proc. natn. Acad. Sci. U.S.A.* **90,** 3675–3679 (1993).
37. Wedegaertner, P. B. & Bourne, H. R. *Cell* **77,** 1063–1070 (1994).
38. Linder, M. E. *et al. J. biol. Chem.* **266,** 4654–4659 (1991).
39. Iniguez-Lluhi, J. A., Simon, M. I., Robishaw, J. D. & Gilman, A. G. *J. biol. Chem.* **267,** 23409–23417 (1992).
40. Bigay, J., Faurobert, E., Franco, M. & Chabre, M. *Biochemistry* **33,** 14081–14090 (1994).
41. West, R. E., Moss, J., Vaughan, M., Liu, T. & Liu, T. Y. *J. biol. Chem.* **260,** 14428–14430.
42. Sullivan, K. A. *et al. Nature* **330,** 758–760 (1987).
43. Hirsch, J. P., Dietzel, C. & Kurjan, J. *Genes Dev.* **5,** 467–474 (1991).
44. Simonds, W. F., Goldsmith, P. K., Codina, J., Unson, C. G. & Spiegel, A.M. *Proc. natn. Acad. Sci. U.S.A.* **86,** 7809–7813 (1989).
45. Conklin, B. R., Farfel, Z., Lustig, K. D., Julius, D. & Bourne, H. R. *Nature* **363,** 274–276 (1993).
46. Hamm, H. E. *et al. Science* **241,** 832–835 (1988).
47. Dratz, E. A. *et al. Nature* **363,** 276–281 (1993).
48. Phillips, W. J. & Cerione, R. A. *J. biol. Chem.* **267,** 17032–17039 (1992).
49. Stryer, L., Hurley, J. B. & Fung, B. K.-K. *Meth. Enzym.* **96,** 617–627 (1983).
50. Kabsch, W. *J. appl. Crystallogr.* **21,** 67–71 (1988).
51. Brunger, A. T. *Acta crystallogr.* **A46,** 46–57 (1990).
52. Brunger, A. T. *X-PLOR Version 3.1 Manual* (Yale University, 1993).
53. Jones, T. A. *et al. Acta crystallogr.* **A47,** 110–119 (1991).
54. Grishin, A. V., Weiner, J. L. & Blumer, K. *Molec. cell. Biol.* **14,** 4571–4578 (1994).
55. Leberer, E. *et al.* EMBO J. **11,** 4805–4813 (1992).
56. Nicholls, A., Sharp, K.A. & Honig, B. *Proteins* **11,** 281–296 (1991).

ACKNOWLEDGEMENTS. We thank M. Capel and L. Berman for access to and help with the X-25 beam line at the NSLS, J. Geiger for assistance during data collection, and E. Neer for making a manuscript available before publication. This work was supported by grants from the NIH to P.B.S. and H.E.H. H.E.H. was also supported by the American Heart Association. D.G.L. and J.S. were Damon-Runyon postdoctoral fellows. The coordinates of the heterotrimer structure will be submitted to the Protein Data Bank.